Optics Letters

Deeply seeing through highly turbid water by active polarization imaging

Fei Liu,[1,2,3] Pingli Han,[1] Yi Wei,[1] Kui Yang,[1] Shengzhi Huang,[1] Xuan Li,[1] Guang Zhang,[2] Lu Bai,[1] and Xiaopeng Shao[1,*]

[1]School of Physics and Optoelectronic Engineering, Xidian University, Xi'an 710071, China
[2]State Key Laboratory of Applied Optics, Chang Chun Institute of Optics, Fine Mechanics and Physics, Chinese Academic of Science, Changchun 130033, China
[3]e-mail: feiliu@xidian.edu.cn
*Corresponding author: xpshao@xidian.edu.cn

Received 31 July 2018; accepted 31 August 2018; posted 6 September 2018 (Doc. ID 339968); published 5 October 2018

We hereby proposed and experimentally demonstrated an active polarization imaging technique, based on wavelength selection, for seeing through highly turbid water where targets are always visually lost. The method was realized by making use of the dependence of light scattering on wavelength in turbid water. Red light illumination was selected to minimize scattering occurring in light propagation and to guarantee accurate estimation of degree of polarization. Experiments demonstrate its contribution to turn targets in highly turbid water from "undetectable" to "detectable."

OCIS codes: (110.0113) Imaging through turbid media; (010.7295) Visibility and imaging; (260.5430) Polarization; (290.5850) Scattering, particles.

https://doi.org/10.1364/OL.43.004903

Optical imaging in underwater environments is drawing increasing attention for applications of target detection and recognition, marine rescue, aquaculture, etc., [1]. Underwater tasks generally depend on effective visual feedback. However, a significant amount of underwater tasks takes place in seas, rivers, lakes, harbors, and coastal areas where visibility is minimal at a fraction of a meter [2]. For example, in three horrible shipwrecks—the Sewol Ferry disaster occurred in 2014, the sinking of Dongfang zhi xing in 2015, and the Phuket boat capsizing in 2018—rescue was a severe challenge due to poor vision in the waters of the wreckages [3,4]. Because of the high turbidity of the accident water, objects at 20 cm away were not visually accessible. Divers are required to descend onto located structures or objects and use their hands to identify victims by tactile examination. In such situations, even visibility in tens of centimeters is crucial to rescuers. Various methods were developed to image in underwater conditions, including time-resolved techniques [5], range-gating technique [6,7], acoustic imaging [8], etc. However, these methods are not available for divers in rescue for too large or too heavy equipment. In contrast, polarization imaging is a more practical way, benefitting from its simple structure and portability. It enables clear underwater imaging, making use of the polarization difference between background light and target light. However, traditional polarization imaging methods often fail when water gets highly turbid [1]. Water with a turbidity of 50 nephelometric turbidity units (NTU) starts to look cloudy and over 500 NTU, appears completely opaque. According to typical levels of natural water, the turbidity of rivers and lakes usually retains an order of tens NTU, and water with a turbidity over 50 NTU is taken as highly turbid water [9]. Imaging results in this kind of water are illustrated in Fig. 1, which are directly captured. The target, a badminton, is located at a distance of 33 cm to the camera. But with water turbidity increased, the target becomes visually lost even at such a short distance. Significant visibility reduction in turbid water stems from the strong absorption and scattering to light by water itself and suspended particles of various origins, for instance, sediments, plankton, algal cells, etc., [10]. Scattering veils the image by redirecting the angle of the photon path, while absorption reduces light intensity by removing the photons permanently from the path [11]. In this context, we develop a wavelength-selection-based active polarization imaging method aiming at providing vision assistance to divers in highly turbid water rescue. It seeks clear vision by suppressing strong scattering in highly turbid water with illumination at a specially selected wavelength and accurately estimating degree of polarization (DoP) by optical correlation.

We can take underwater images as a sum of backscattered light and target light. Backscattered light and target light are

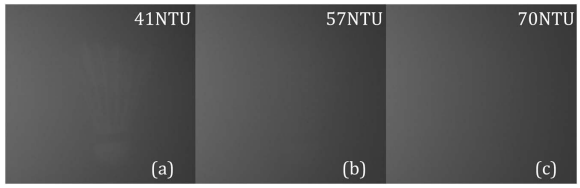

Fig. 1. Directly captured images in turbid water at 41 NTU, 57 NTU, and 70 NTU.

measured for two polarization channels: orthogonal to the backscatter's polarization state $I_{\min}$ and parallel to the backscatter's polarization state $I_{\max}$ [12]. A clear underwater image and backscattered light image can then be modeled by Eq. (1):

$$I_{\text{obj}} = \frac{1}{p_{\text{scat}} - p_{\text{obj}}}[I_{\max}(1 + p_{\text{scat}}) - I_{\min}(1 - p_{\text{scat}})]$$
$$I_{\text{sca}} = \frac{1}{p_{\text{scat}} - p_{\text{obj}}}[I_{\max}(1 - p_{\text{obj}}) - I_{\min}(1 + p_{\text{obj}})], \quad (1)$$

where p_{scat} is the DoP of backscattered light, and p_{obj} is DoP of target light. Traditional polarization imaging often fails when water gets turbid [1]. Here we will analyze how the turbidity increases affect polarization imaging quality from the point of image noise amplification. According to Eq. (1), final detected images rely heavily on the two measurements $I_{\max}$ and $I_{\min}$. Suppose these two measurements are statistically independent with noise variances $\sigma^2_{\max}$ and $\sigma^2_{\min}$, respectively. Then the noise variance in the final detected image I_{obj} is given by Eq. (2) [12]:

$$\sigma^2_{\text{obj}} = \left(\frac{\partial I_{\text{obj}}}{\partial I_{\max}}\right)^2 \sigma^2_{\max} + \left(\frac{\partial I_{\text{obj}}}{\partial I_{\min}}\right)^2 \sigma^2_{\min}$$
$$= \left(\frac{1 + p_{\text{scat}}}{p_{\text{obj}} - p_{\text{scat}}}\right)^2 \sigma^2_{\max} + \left(\frac{1 - p_{\text{scat}}}{p_{\text{obj}} - p_{\text{scat}}}\right)^2 \sigma^2_{\min}. \quad (2)$$

It is obvious that with p_{scat} approaching p_{obj}, σ^2_{obj} increases rapidly. For a more straightforward explanation, we take the case $\sigma_{\max} = \sigma_{\min} = \sigma_0$. Then Eq. (2) is simplified to

$$\sigma^2_{\text{obj}} = 2\left[\frac{1 + p^2_{\text{scat}}}{(p_{\text{obj}} - p_{\text{scat}})^2}\right]\sigma^2_0. \quad (3)$$

Figure 2(a) depicts $\sigma_{\text{obj}}/\sigma_0$ as derived in Eq. (3). In any case, $\sigma_{\text{obj}} > \sigma_0$, i.e., the noise is amplified, especially when $p_{\text{obj}} \approx p_{\text{scat}}$. Data in Fig. 2(b) show p_{obj}, p_{scat} and their difference $p_{\text{scat}} - p_{\text{obj}}$ as a function of water turbidity. p_{obj} increases with the turbidity increase, while p_{scat} retains a small fluctuation, leading to decreasing difference between p_{obj} and p_{scat}, which finally results in strongly amplified noise covering over target information.

In turbid water, p_{obj} increase results from greatly increased scattering events due to the growth in number of floating particles. The more turbid the water becomes, the more scattering events happen. Strongly backscattered light veils the target and at the same time enhances DoP of light in the target region, i.e., p_{obj} increases. Petzold measured light scattering in very clear seawater, costal seawater, turbid harbor water, and pure seawater. Partial data are shown in Fig. 3(a) [13], indicating that scattering gets significantly stronger as water turbidity increases. Strong scattering also accounts for the rapid vision loss in highly turbid water.

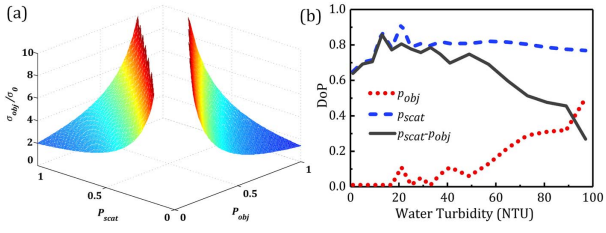

Fig. 2. (a) Noise standard deviation σ_{obj} as a function of σ_0, p_{obj} and p_{scat}; (b) p_{obj} as a function of water turbidity.

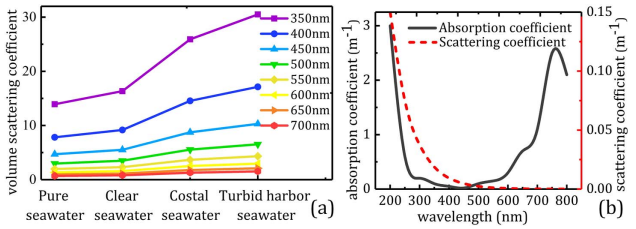

Fig. 3. (a) Measured VSF (volume scattering function) in four different water conditions [13]; (b) measured absorption and scattering coefficients of pure seawater.

To image through highly turbid water, it is crucial to suppress the strong scattering effect. In natural waters, both waterbody and suspended particles contribute to light scattering. Theoretically, natural waters' scattering coefficient is determined by the scattering coefficients of each component. Practically, however, it is not possible to measure the scattering properties of each individual scattering component, and thus scattering events can be grouped into Rayleigh scattering and Mie scattering based upon comparison between the scattering particles and wavelength of incident light [14,15]. Light scattering caused by pure water performs more like Rayleigh scattering. Its volume scattering function (VSF), defined as the scattered radiant intensity oriented into a scattering angle, is illustrated by Eq. (4) [16]:

$$\beta_w(\psi;\lambda) = \beta_w(90°;\lambda_0)\left(\frac{\lambda_0}{\lambda}\right)^{4.32}(1 + 0.835\cos^2\psi), \quad (4)$$

where λ_0 denotes a reference wavelength, and ψ is the solid angle. As for scattering caused by floating particles, Kopelevich and Mezhericher developed a double-parameter model that divides particles into small particles (<1 μm) and large particles (>1 μm). The particle VSF is expressed by Eq. (5):

$$\beta_p(\psi;\lambda) = v_s\beta_s(\psi)\left(\frac{\lambda_0}{\lambda}\right)^{1.7} + v_l\beta_l(\psi)\left(\frac{\lambda_0}{\lambda}\right)^{0.3}, \quad (5)$$

where v_s and v_l are concentrations of small particles and large particles, respectively; β_s and β_l are VSF of small particles and large particles, respectively [17].

The VSFs in Eqs. (4) and (5) suggest the possible scattering events light goes through while propagating in water. It is worth noting that scattering caused by both water and particles is wavelength dependent. Smith and Baker measured the absorption coefficients and scattering coefficients of pure seawater [18]. Measured data validated the dependence of scattering on wavelength. In visible-light range, scattering decreases with wavelength increase, as shown in Fig. 3(b). Based upon this wavelength-dependent fact, we propose a wavelength-selection-based polarization imaging method to image through highly turbid water with red light illumination, by which the scattering events could be effectively reduced.

Figure 4 shows the experimental layout of the method. Particularly, red light illumination is required. To mimic the scattering properties of natural water, the solution of 260 L tap water and milk is used to simulate natural turbid water in a 250 (length) cm × 50 (width) cm × 40 (height) cm water tank. The back wall of the tank is antireflection coated to prevent reflection from the back wall to the camera. A red LED light source, M625L3, from Thorlabs is used for illumination

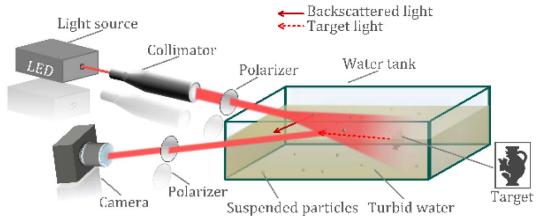

Fig. 4. Experimental arrangement for imaging in highly turbid water.

at a wavelength centered at 625 nm. The wavelength is determined based upon the scattering and absorption coefficients distribution in Fig. 3(b) at which the scattering and absorption effects reach a good balance. A polarizer in front of the light source ensures linear polarization to impinge upon the medium. Two polarization images I_{max} and I_{min} are first taken and exploited for clear imaging by Eq. (1) where p_{scat} and p_{obj} are also necessary. p_{scat} is achieved by selecting an area without any object in I_{max} and I_{min} and computing its DoP by Eq. (6) [12]:

$$p_{scat} = \frac{I_{max} - I_{min}}{I_{max} + I_{min}}, \tag{6}$$

while for estimation of p_{obj}, Eq. (6) is not available with backscattered light veiling the target. Here, we discuss an approach to estimate p_{obj} based on the information similarity between backscattered light I_{scat} and target light I_{obj}. To quantify the similarity, we exploit the optical correlation theory, more precisely, the matched filter-Vanderlgut correlator. It first transforms a target image into the Fourier domain, builds a filter with a reference image, then conducts the filtering in Fourier domain, and finally generates a correlation plane. The filter used in the Fourier domain determines the final similarity quantification. Here, we adopt a phase-only filter (POF) $H(\mu, \upsilon)$ defined by Eq. (7):

$$H(\mu, \upsilon) = R^*(\mu, \upsilon)/|R(\mu, \upsilon)|, \tag{7}$$

where μ and υ are the coordinates in the frequency plane, $R(\mu, \upsilon)$ is the spectrum of the backward scattering image, and * denotes the complex conjugate [19]. This filter is very discriminating with a sharp peak. The final correlation plane distributes as Eq. (8) shows:

$$u(x, y) = \frac{1}{4\pi^2} \iint_{-\infty}^{\infty} T(u, v) \frac{R^*(u, v)}{|R(u, v)|} e^{i(ux+vy)} \mathrm{d}u\mathrm{d}v. \tag{8}$$

Here, we set I_{scat} as the reference image and I_{obj} as the target image, as shown in Fig. 5.

As an example, Fig. 6 plots the correlation peak (CP) values for every potential p_{obj} in three different water conditions with turbidities of 41 NTU, 57 NTU, and 70 NTU. A narrow and

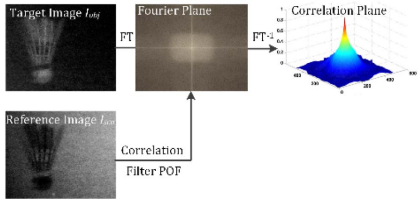

Fig. 5. Synoptic diagram of VL; FT denotes Fourier transform.

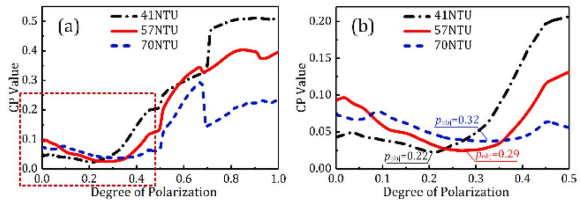

Fig. 6. (a) CP value as a function of p_{obj} in three different water conditions with a turbidity of 41 NTU, 57 NTU, and 70 NTU; (b) zoomed-in view of the marked part of plot (a).

high CP indicates good similarity between I_{scat} and I_{obj}. Here in this study, we are looking for I_{scat} and I_{obj} with the least similarity. p_{obj} is then determined by searching the minimum CP value in each curve in Fig. 6. Then the estimated p_{obj} values are used in Eq. (1) to estimate clear underwater images.

Figure 7 shows images of the target inside highly turbid water with turbidities of 41 NTU and 70 NTU, respectively. Figures 7(a1) and 7(b1) are captured directly by a camera, Figs. 7(a2) and 7(b2) are results from the traditional polarization imaging approach, and Figs. 7(a3) and 7(b3) are the finally detected results by the proposed method. The increase in turbidity leads to stronger light scattering. When water turbidity reaches 70 NTU, the target inside is already invisible in the directly captured image at a 33 cm detection distance. This demonstrates the necessity for divers to identify targets by tactile examination in some conditions, since even at a short range, targets are still not visually accessible. Even the traditional polarization imaging method cannot provide effective improvement, as shown in Figs. 7(a2) and 7(b2). In contrast, in Figs. 7(a3) and 7(b3), we can tell that the proposed method increases the visibility significantly. In water with a 41 NTU turbidity, the proposed method is almost unaffected by strong scattering. It provides a clear underwater image of the target with distinct details and hardly no backscattered light. Even in 70 NTU turbid water, it still can provide abundant target information, including distinct outlines and distinguishable textures. This improvement benefits from the impaired scattering effect with red light illumination. In detail, within the same detection distance, red light experiences many fewer scattering events than visible light at other wavelengths, which enables the backscattered light to retain a relatively high value of p_{scat}. Further use of p_{scat} in Eq. (3) makes a more accurate estimation. Finally, a clear target image is achieved. Although red light cannot last long due to water absorption, in highly turbid water,

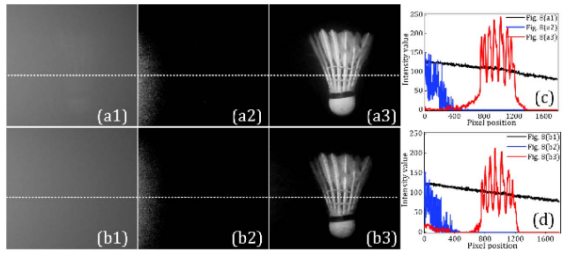

Fig. 7. (a1) and (b1) Directly captured images in 41 NTU and 70 NTU turbid water; (a2) and (b2) results from traditional polarization imaging method; (a3) and (b3) finally detected images by the proposed method; (c) and (d) intensity profiles along the white dotted lines in (a1)–(b3) (see Visualization 1).

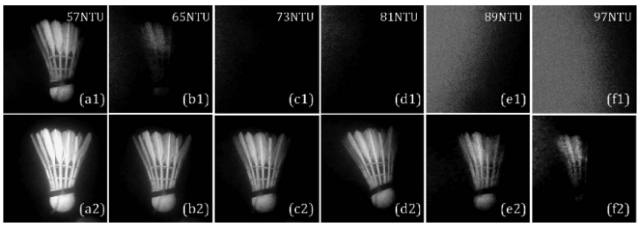

Fig. 8. Detection results with blue light illumination (a1) to (f1), and from the proposed method (a2) to (f2) in water with gradually varied turbidity.

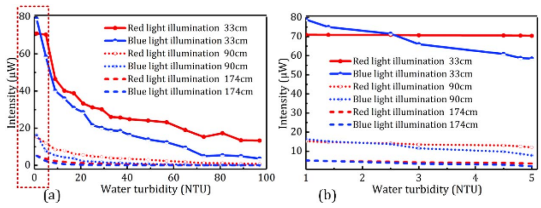

Fig. 9. Measured light intensity at a 33 cm, 90 cm, and 174 cm distance.

it provides a beneficial balance between the range and vision. Even the range before it is totally attenuated is of great value for target detection in highly turbid water.

As an attempt to visualize the improvement of the proposed method in imaging through highly turbid water, the curves in Figs. 7(c) and 7(d) are plotted, which represent the intensity profiles along the white dotted lines crossing the middle of Figs. 7(a1)–7(b3). For example, no obvious target information is indicated with the selection of the directly captured image in 70 NTU turbid water. The contrast, defined by the maximum intensity of the target and minimum intensity of the background divided by their sum, is 0.76 for Fig. 7(b1). By comparison, noticeable target information is observed as an obvious bump in the intensity profile of the detected image by the proposed method, as we expected. This profile clearly shows the target location and a considerable contrast improvement. After calculation, it turns out the contrast is enhanced to an expectable value of 2.43 for Fig. 7(b3).

Generally, blue light is thought to be able to travel a longer distance in water than light in other wavelengths. It is widely used in underwater target detection. As a comparison, experiments with blue light (M470L3, wavelength centered at 470 nm) illumination are performed, and results are exhibited in Figs. 8(a1)–8(f1). With water turbidity increasing, image quality rapidly decays. The target is totally lost when water turbidity reaches 73 NTU, while the proposed method keeps providing substantial target information with water turbidity increasing to nearly 100 NTU, as shown in Figs. 8(a2)–8(f2). The failure of blue light is partially caused by complex scattering in highly turbid water where scattering dominates light attenuation. Research demonstrated clear water retains the minimum absorption coefficient to blue light, making blue color the dominated color of clear waters. However, highly turbid water is abundant in scattering particles, where blue light cannot keep its advantage due to strong scattering. The proposed method gave up blue light illumination to avoid this problem, and obtained positive results. Although red light can still be absorbed by waterbody, its experience with less scattering events enables a longer propagation distance. Data in Fig. 9 make a sound demonstration, presenting light intensity variation with water turbidity measured at three distances: 33 cm, 90 cm, and 174 cm. In clear water, blue light can provide stronger illumination at all locations. Interestingly, with water getting turbid, red light starts to present a growing lead in light intensity. It reveals that turbid water differs from clear water in optical properties with much stronger scattering. The proposed method makes full use of the difference to improve imaging quality in turbid water.

In conclusion, this Letter introduced an active polarization imaging method based upon wavelength selection to provide vision assistance to divers for rescue in highly turbid water. It takes advantage of the dependence of light scattering on wavelength in turbid water where red light makes a good balance between range and vision. Notable improvements can be expected even when targets are visually lost. The method's major contribution is to turn targets from "undetectable" into "detectable." It is of great value for underwater rescue in turbid lakes, rivers, or harbor areas where even poor visibility is hardly achievable, and tactile examination by divers is needed to find victims.

Funding. National Natural Science Foundation of China (NSFC) (61475123, 61705175); China Postdoctoral Science Foundation (2017M613063).

REFERENCES

1. Y. Y. Schechner and N. Karpel, IEEE J. Ocean. Eng. **30**, 570 (2005).
2. W. Hou, Opt. Lett. **34**, 2688 (2009).
3. B. Laurie and W. C. Han, "Chinese ship that sank in Yangtze River was cited for safety issues," (The Wall Street Journal, June 3, 2015).
4. J. Kim and C. Yoo, "More than 300 people missing after South Korea ferry sinks—Coast Guard," (Reuters, April 16, 2014).
5. J. Tong, W. Tan, J. Si, Y. Yang, W. Yi, F. Chen, and X. Hou, J. Appl. Phys. **109**, 123104 (2011).
6. D. M. Kocak, F. R. Dalgleish, F. M. Caimi, and Y. Y. Schechner, Mar. Technol. Soc. J. **42**, 52 (2008).
7. C. Tan, G. Seet, A. Sluzek, X. Wang, C. T. Yuen, C. Y. Fam, and H. Y. Wong, Opt. Express **18**, 21147 (2010).
8. W. Hou, E. Jarosz, S. Woods, W. Goode, and A. Weidemann, Opt. Express **21**, 4367 (2013).
9. E. Myre and R. Shaw, *The Turbidity Tube: Simple and Accurate Measurement of Turbidity in the Field* (Michigan Technological University, 2006).
10. G. A. Weyhenmeyer, T. Blenckner, and K. Pettersson, Limnol. Oceanogr. **44**, 1788 (1999).
11. S. A. Kartazayeva, X. Ni, and R. R. Alfano, Opt. Lett. **30**, 1168 (2005).
12. T. Treibitz and Y. Y. Schechner, IEEE Trans. Pattern Anal. Mach. Intell. **31**, 385 (2009).
13. T. J. Petzold, *Volume Scattering Functions for Selected Ocean Waters* (Scripps Institute of Oceanography La Jolla Ca Visibility Lab, 1972).
14. C. Gabriel, M.-A. Khalighi, S. Bourennane, P. Leon, and V. Rigaud, *2nd IEEE Workshop on Optical Wireless Communications* (2011).
15. K. Clays and A. Persoons, Phys. Rev. Lett. **66**, 2980 (1991).
16. C. D. Mobley, *Light and Water: Radiative Transfer in Natural Waters* (Academic, 1994).
17. O. Kopelevich and E. Mezhericher, Izv. Atmos. Ocean. Phys. **19**, 144 (1983).
18. R. C. Smith and K. S. Baker, Appl. Opt. **20**, 177 (1981).
19. M. Dubreuil, P. Delrot, I. Leonard, A. Alfalou, C. Brosseau, and A. Dogariu, Appl. Opt. **52**, 997 (2013).